Melt Processing of Poly(L-Lactic Acid) in the Presence of Organomodified Anionic or Cationic Clays

Vimal Katiyar,[1] Nathalie Gerds,[2,3] Christian Bender Koch,[2] Jens Risbo,[3] Hans Christian B. Hansen,[2] David Plackett[1]

[1]*Solar Energy Programme, Risø National Laboratory for Sustainable Energy, Technical University of Denmark, Roskilde DK-4000, Denmark*
[2]*Faculty of Life Sciences, Department of Basic Sciences and Environment, University of Copenhagen, Thorvaldsensvej 40, Frederiksberg DK-1871, Denmark*
[3]*Faculty of Life Sciences, Department of Food Science, University of Copenhagen, Rolighedsvej 30, Frederiksberg DK-1958, Denmark*

Received 15 September 2010; accepted 13 December 2010
DOI 10.1002/app.33984
Published online 19 April 2011 in Wiley Online Library (wileyonlinelibrary.com).

ABSTRACT: Poly(L-lactic acid) (PLA) films are in use for various types of food packaging; however, a wider range of applications would be possible if the barrier properties of these films could be improved. To make such improvements, combinations of PLA with two nanofillers, laurate-intercalated Mg-Al layered double hydroxide (LDH-C_{12}) and a cationic organomodified montmorillonite (MMT) clay (Cloisite® 30B), were investigated. The dispersion of these fillers in PLA by melt processing was explored using two methods, either by mixing the nanofillers with PLA granulate immediately before extrusion or by preparation and subsequent dilution of PLA-nanofiller masterbatches. After melt processing of these materials, PLA molecular weight, thermal stability, film transparency, morphology, and permeability characteristics were determined. Direct addition of LDH-C_{12} drastically reduced the PLA molecular weight. Although this reduction in molecular weight was still very significant, it was less when a PLA/LDH-C_{12} masterbatch was processed. In contrast, there was no significant reduction in PLA molecular weight when processing with Cloisite® 30B. However, film transparency was compromised when either LDH or MMT nanofillers were used. Evidence from DSC analyses showed a significant increase in heat of fusion when LDH-C_{12} was dispersed in PLA compared with Cloisite® 30B, likely indicating a difference in nucleating properties. Complementary optical purity analyses suggested that racemization as a result of processing could influence the PLA crystallinity as determined by DSC in certain cases. A reduction in thermal stability when incorporating LDH-C_{12} could be a direct result of PLA molecular weight reduction. XRD and TEM analyses showed that both Cloisite® 30B- and LDH-C_{12}-based PLA composites yielded exfoliated and intercalated morphologies, but nanofiller agglomeration was also seen when LDH-C_{12} was used. PLA/Cloisite® 30B nanocomposite films exhibited significant enhancement in oxygen and water vapor barrier properties, but no such improvement was found in PLA/LDH-C_{12} nanocomposite films. J Appl Polym Sci 122: 112–125, 2011

Key words: poly(L-lactic acid); layered double hydroxides; nanocomposites; *in-situ* ring-opening polymerization; processing

INTRODUCTION

In recent years, the development and use of bioderived, biodegradable polymers has attracted increasing interest because of their potential contribution in terms of reduced fossil-fuel dependence and the environment.[1,2] Among the polymers in this category, poly(lactic acid) (PLA) has been identified as a good candidate to partially substitute for petroleum-derived polymers such as polypropylene, polystyrene, or polyethylene(terephthalate)[3,4] in some uses. The main advantage of PLA is that it decomposes rapidly and completely in a composting environment, which makes it a potentially suitable replacement material for nondegradable polymers in applications such as packaging.[5,6] In particular, there is interest in PLA as a film for food packaging applications.[2,7]

The main commercial route to PLA production is presently through ring-opening polymerization of L-lactide. Lactides are stereoisomers which exist in either L-, D-, meso- or racemic chiral forms and L-lactide can be synthesized from lactic acid, obtained by fermentation of starch from agricultural feedstocks (e.g., corn, sugar beet, sugar cane[8–10]). The mechanical, thermal, and biodegradation properties of PLA are dependent on the stereosequence of PLA repeat units. For example, PLA in which the backbone carbons have the same stereo-configuration (either R or S) is isotactic and crystallizable. The crystallinity of PLA is important for its load-bearing and gas barrier

Correspondence to: D. Plackett (dapl@risoe.dtu.dk).
Contract grant sponsor: Danish Strategic Research Council (NanoPack Project).

properties as well as its degradation behavior and hence its suitability for specific packaging applications. To modify the crystallization behavior of PLA and therefore the related polymer properties, the concept of stereocomplex formation using varying amounts of poly(D-lactic acid) (PDLA) as a nucleating agent in poly (L-lactic acid) (PLLA) has been demonstrated.[11] Subsequently, there have been studies on dispersing PLA stereocomplexes, talc, fullerenes, or clays as nucleating agents which can accelerate crystallization in PLA films.[12]

Many reports are now available in which PLA has been filled with clays consisting of two-dimensional sheets with nanoscale thickness (e.g., $\sim$ 1 nm for montmorillonite (MMT) clay) and therefore with a high aspect ratio.[5,13–17] The resulting PLA nanocomposite materials exhibit improved stiffness, toughness, resistance to heat, fire and ignition, as well as higher gas barrier properties.[5] These property improvements are achieved through interaction between inorganic surfaces of nanoclays and the PLA matrix. When the polymer intercalates between the layered sheets of the clay, mechanical properties are enhanced due to production of a well-ordered multilayer morphology composed of alternating polymer matrix and inorganic layers.[18] In contrast, when the polymer is unable to intercalate between the clay sheets, a phase-separated macrocomposite is obtained and significant property enhancements are not achieved.[6]

PLA-clay nanocomposites are potentially useful new packaging materials with desirable mechanical and permeability properties, providing that the nanoclays can be well dispersed in the polymer matrix. For this reason, the final properties depend on the technique by which clays are dispersed in the polymer. In the case of melt-extruded PLA with organically modified MMT clays, significant modification of the crystallization behavior, material properties and biodegradation has been demonstrated.[15,19,20] Clay addition can also improve the heat distortion temperature, which is an important characteristic for the successful use of PLA in packaging.[20] In terms of clay dispersion, it has been shown that better exfoliation can be achieved when the clay organomodifier is functionalized and that nonfunctionalized modifiers tend to produce intercalated morphologies.[21]

Although there have been many studies on the use of MMTs as polymer nanofillers, layered double hydroxides (LDHs), typically synthesized in the laboratory, have been much less studied.[22,23] LDHs are brucite-like layer materials, having anionic counterions in the gallery space. The general chemical formula is $[M^{2+}_{1-x}\ M^{3+}_{x}\ (OH)_2]^{x+}\ A^{m-}_{x/m}\ .nH_2O$ where M^{2+} is a divalent cation, M^{3+} is a trivalent cation, and A^- is an interlamellar anion with charge m.[24] To utilize LDHs in thermoplastic processing, the preparation of organomodified LDH is required so as to achieve compatibility with more hydrophobic thermoplastics. In the *in-situ* polymerization method, a monomer is inserted in the LDH interlayer space (galleries) and this step is followed by polymerization yielding polymer-LDH nanocomposites.[25] This technique is effective because, instead of large polymer chains, small monomers can readily be inserted into the galleries, leading to LDH hydrophobicity and greater compatibility with hydrophobic polymers.[26–28] Recently, PLA nanocomposites incorporating LDHs have been reported. For example, melt mixing of PLA with dodecyl sulfate-modified LDH was performed using a single-screw extruder.[29] Chiang et al.[30] prepared PLA-modified LDH and subsequently dispersed this LDH into bulk PLA solution to obtain a PLA-LDH nanocomposite. Dagnon et al.[31] produced a PLA nanocomposite using an LDH functionalized with ibuprofen and a solution casting technique. In this case, the polymer storage modulus, tensile modulus, and ultimate tensile strength were all improved, although LDH addition also reduced the thermal stability of the PLA. Many reports have discussed the general mechanical and barrier properties of PLA nanocomposites.[7,32–39]

In the study described here, PLA/clay compounding and film processing was investigated on the scale of a few kilograms as a prelude to further studies aimed at more demanding applications of PLA in food packaging. An organomodified LDH and a commercial MMT (Cloisite® 30B) were evaluated and their processibility was compared. Clay dispersion behavior and composite properties were investigated in materials prepared using either dry mixing of PLA granulates with clays before melt processing or by preparation and subsequent dilution of PLA/clay masterbatches.

EXPERIMENTAL

Materials

PLA (NatureWorks LLC Ingeo™ 2003D) was dried at 100°C for $\sim$ 4 h prior to use. L-Lactide (>98%), tin (II) 2-ethyl hexanoate (>95%), toluene (>99.9% HPLC grade), dichloromethane (>99.9%), tetrahydrofuran (THF; >99.9% HPLC grade), and chloroform (>99.8%) were purchased from Sigma Aldrich, Denmark and utilized for the preparation of masterbatches. Methanol (>99.9%) was used as supplied by J. T. Baker Chemicals, Denmark. L-lactide was recrystallized three times in toluene, which had been previously dried using fresh 4 Å molecular sieve (Bie and Berntsen A/S, Denmark), and then dried under vacuum at 70°C for 4 h. Laurate-modified LDH(LDH-C_{12}) was synthesized using lauric acid

from Aldrich Chemie GmbH, Germany, in combination with magnesium nitrate and aluminum nitrate from Merck KGaA, Germany. All the commercial chemicals were analytically pure grades. Organomodified MMT was obtained in the form of Cloisite® 30B from Southern Clay Products, Gonzales, Texas.

Synthesis of LDH-C_{12}

LDH carbonate (LDH-CO_3) was synthesized by a coprecipitation method similar to that previously reported by Miyata.[40] In a typical synthesis, 1.5 L of an 0.67*M* aqueous solution of $Al(NO_3)_3{\cdot}9H_2O$ was slowly added over 8 h to a 15-L vessel containing 5 L of an 0.6*M* aqueous solution of $Mg(NO_3)_2{\cdot}6H_2O$. The pH of the reaction mixture was adjusted to 9 by dropwise addition of mixed 2*M* NaOH and 0.2*M* Na_2CO_3 solutions, and the suspension was constantly stirred at room temperature over a further 12-h period. The precipitate was isolated by repeated centrifugation, washed three times using double-deionized water and freeze dried.

To produce LDH-C_{12}, the synthesized LDH-CO_3 was first calcined to form a mixed metal oxide (MMO) by heating for 5 h in a muffle furnace at 500°C. In the next step, 10 L of a 30 : 70 EtOH-H_2O (v/v) sodium laurate solution was prepared by neutralization of lauric acid (0.1*M*) solution with sodium hydroxide to pH 9. The laurate solution was further flushed with argon at a flow rate of $\sim$ 50 mL min^{-1} for 5 h to remove carbon dioxide. Subsequently, the MMO (150 g) was dispersed into the sodium laurate solution under argon, and the suspension was then stirred overnight at room temperature. The final product was separated by repeated centrifugation, cleaned with an alkaline ethanol-water mixture (1 : 1), and freeze dried. The solid was further dried in a vacuum oven at 110°C to minimize contamination by carbon dioxide.

Synthesis of PLA/Cloisite® 30B and PLA/LDH-C_{12} nanocomposite masterbatches

PLA/Cloisite® 30B and PLA/LDH-C_{12} masterbatches were produced by an *in-situ* intercalative ring-opening polymerization (ROP) method. Mixtures of Cloisite® 30B or LDH-C_{12} and L-lactide were first prepared by dispersion of the clays (50% by wt) into solutions of L-lactide (10% w/v) in dichloromethane with vigorous stirring for 24 h at room temperature. Subsequently, dry Cloisite® 30B/lactide or LDH-C_{12}/lactide mixtures were obtained after evaporation of the solvent under reduced pressure at room temperature. Each mixture was then charged in a round-bottomed flask and tin (II) 2-ethyl hexanoate catalyst was added to obtain a lactide:catalyst molar ratio in the range of 200–500. The solvent and any gaseous impurities were removed and the reactor was sealed under high vacuum. Polymerization was carried out at 160°C for 2 h in the case of the Cloisite® 30B/lactide mixture or at 140°C for 2 h in the case of the LDH-C_{12}/lactide mixture. The effect of clay loadings in the 10–60 wt % range was first investigated on a small scale and, on the basis of this work, 50 wt % loading was selected for both the Cloisite® 30B and LDH-C_{12} masterbatches.

Processing of PLA and PLA nanocomposite granulates

PLA and Cloisite® 30B or LDH-C_{12} and their respective masterbatches containing 50 wt % clay were compounded into pellets with a target loading of 5 wt % clay using a twin-screw corotating extruder (Jiangyu Xinhua Plastics Machinery, Wuxi, Shanghai, China) with an attached three-hole strand die (3 mm), cooling bath, and pelletizer. The extruder was configured with a 35 mm barrel diameter and L/D ratio of 44 : 1. The temperature profile in the extruder was set in seven zones and monitored at 150°C in the feed zone with sequential temperatures of 189, 175, 195, and 207°C in the metering zone. The die zone temperature was set at 180°C, but actual readings were maintained at $\sim$ 200–205°C because of shear-induced heating in the extruder. The feed rate was set at 18 kg/h by adjusting the screw speed to 40 rpm. The Cloisite® 30B or LDH-C_{12} fillers or their PLA masterbatches were mixed well with dry PLA pellets by tumbling preweighed amounts in sealed containers before feeding into the extruder. Nanocomposite strands were pulled through a water bath at ambient temperature and, after removing the surface water by air knife, the strands were pelletized. Unfilled PLA pellets were processed under the same conditions so that this reference material would have the same thermal history as the nanocomposite pellets.

Processing of PLA and PLA/clay nanocomposite films

Pellets of the various materials were dried for 2 h at 100°C to remove residual moisture from the pelletizing process. Reference unprocessed PLA pellets, extruded PLA pellets, and compounded PLA/LDH-C_{12} or PLA/Cloisite® 30B nanocomposite pellets were then converted into films. Each set of pellets was loaded into a 30-mm barrel diameter single-screw extruder with L/D ratio of 30 : 1 (Labtech Engineering Company, Bangkok, Thailand). The screw speed was set at 155 rpm, and material was fed to the extruder by means of a primary volumetric feeder. The temperature profile of the extruder was set in five zones and also at the die head. The

TABLE I
Nomenclature of the PLA and PLA Nanocomposite Materials

Sample code	Clay/loading (%)[a]	Description
PLA-G	–	NatureWorks® 2003D PLA granulate
PLA-GF	–	Film from PLA-G granulate
PLA-P	–	PLA-G converted to extruded pellets
PLA-PF	–	Film from PLA-P pellets
PLA-P1	4.5% Cloisite® 30B	PLA and Cloisite® 30B mixed and converted to extruded pellets
PLA-PF1	4.5% Cloisite® 30B	Film from PLA-P1 pellets
PLA-P2	5.3% Cloisite® 30B	Extruded pellets from PLA-Cloisite® 30B masterbatch diluted with PLA-G
PLA-PF2	5.3% Cloisite® 30B	Film from PLA-P2 pellets
PLA-P3	5.3% LDH-C_{12}	PLA and LDH-C_{12} mixed and converted to extruded pellets
PLA-PF3	5.3% LDH-C_{12}	Film from PLA-P3 pellets
PLA-PF3–1	1.8% LDH-C_{12}	Film from PLA-P3 pellets diluted ×3 with PLA-G
PLA-P4	5.5% LDH-C_{12}	Extruded pellets from PLA/LDH-C_{12} masterbatch diluted with PLA-G
PLA-PF4	5.5% LDH-C_{12}	Film from PLA-P4 pellets
PLA-PF4–1	1.8% LDH-C_{12}	Film from PLA-P4 pellets diluted ×3 with PLA-G

[a] Target loadings were 5% in each case but values shown in the table indicate loadings estimated by TGA analysis.

temperature profile for PLA and PLA/Cloisite® 30B nanocomposite pellets was set to 210–220°C across the five zones and at 205°C in the die zone. The temperature profile for PLA/LDH-C_{12} nanocomposite pellets was fixed at ~ 160°C in the barrel and at ~ 175°C in the die zone. The flow rate of molten PLA with or without clay filler was ~ 1.9 m/min across the width of the die (20 cm). Extruded films were collected on a chilled and highly polished turning roll and quenched on the contact side before transfer to a second roll for cooling on the other side. Each extruded film was passed through rollers at ~ 1.6 m/min to obtain ~ 400 μm-thick film and then finally rolled on to a winder at ~ 60 rpm. A summary of the chosen nomenclature for granulates and films is presented in Table I.

Compound and film characterization

PLA and PLA nanocomposite pellets and films were characterized using gel permeation chromatography (GPC), differential scanning calorimetry (DSC), thermogravimetric analysis (TGA), optical polarimetry, UV/visible spectroscopy, X-ray diffraction (XRD), and transmission electron microscopy (TEM). In addition, the oxygen and water vapor (WV) permeability of the films was measured.

Gel permeation chromatography

GPC was carried out using a Shimadzu LC-10AD GPC with PL-gel 5 μm Mixed-C and Mixed-D columns in series and a Viscotek RI Detector. Polystyrene standards up to 680,000 Da were dissolved in THF and used for calibration. Samples were analyzed using injection volumes of 100 μL and with THF eluent at a flow rate of 0.5 mL/min. To avoid column contamination, 25 mg samples were dissolved in 5 mL of chloroform and then filtered after 24 h using 0.45 μm Whatman® filters before GPC analysis.

Thermogravimetric analysis

A TA Instruments Q 500 TGA instrument was utilized for thermal stability studies on PLA and PLA-nanofiller samples. TGA analyses were performed from ambient temperature up to 600°C under nitrogen at a heating rate of 10°C/min.

Differential scanning calorimetry

The glass transition temperature (T_g), melting temperature (T_m), enthalpy of melting (ΔH_m), and crystallinity (X_c) of unfilled PLA and PLA-nanofiller mixtures were determined under nitrogen using a TA Instruments Q 1000 system in the temperature range 25–200°C with heat-cool-heat scans at 10°C/min. For the determination of X_c of neat PLA and the PLA/LDH-C_{12} or PLA/Cloisite® 30B mixtures, the melt enthalpy of 100% crystalline PLA was taken as $\Delta H_f^0 = 93$ J/g.[41] After considering the effect of clay loading (ϕ), room temperature crystallinity was calculated using eq. (1).

$$X_C = \frac{\Delta H_f}{(1-\phi)\Delta H_f^0} \times 100\% \quad (1)$$

Optical polarimetry

The specific optical rotation of the PLA granulates, PLA film and PLA/clay nanocomposite films was measured in chloroform (1 g/dL) at 25°C using a JASCO 1000 polarimeter at a wavelength of 589 nm. To avoid the interference of clay particles during optical measurements, ~ 200 mg samples were dissolved in 20 mL of chloroform with stirring for 48 h

and the suspensions were then filtered using 0.45 μm Whatman filters before analysis. The weight of PLA present in the case of PLA nanocomposite film samples was calculated by excluding the weight fraction of clay. Thereafter, we estimated the optical purity (%L-content) and subsequently, calculated mole fractions of L-lactyl (X_L) and D-lactyl (X_D) units using eq. (2).[42] The specific optical rotation values [α] of pure L-PLA or D-PLA are reported to be −156 and +156, respectively.[43]

$$X_D = [D-\text{unit}]/([D-\text{unit}] + [L-\text{unit}]) = [[\alpha] - (-156)]/[156 - (-156)] \quad (2)$$

UV–visible spectroscopy

Transparency measurements were carried out using a Varian Inc. Cary 5 UV/Visible spectrophotometer in the wavelength range 200–900 nm with scan rate of 5 nm/s and a spectral bandwidth of 2 nm.

X-ray diffraction

XRD analyses were performed on powder samples of Cloisite® 30B, LDH-CO_3, LDH-C_{12}, and PLA nanocomposites using a Siemens D5000 X-ray diffractometer equipped with a Co tube and a diffracted beam monochromator, allowing selection of Co K_α radiation of wavelength (λ) = 0.1789 nm. The instrument was operated at 40 kV/40 mA, and samples were scanned in continuous mode with a scan rate of 0.4–2 degrees min^{-1} in the range 2–30° 2θ.

Transmission electron microscopy

The morphology of PLA nanocomposites was examined by performing bright field imaging using a Tecnai G^2 12 transmission electron microscope. The microscope was operated at an accelerating voltage of 200 kV. Ultrathin sections of PLA nanocomposites (~ 80 nm thickness) were prepared at room temperature using a Leica® EM UC6 ultramicrotome (Leica Microsystems, Wetzlar, Germany) equipped with a glass knife.

Permeability measurements

The oxygen permeability of sample films was measured at 23°C ± 0.03°C and 50% ± 2% RH using a PBI-Dansensor (Ringsted, Denmark) OPT 5000 oxygen permeability tester containing a ceramic solid-state oxygen sensor. Dry nitrogen containing less than 0.1 ppm oxygen (Alphagaz 2, Air-Liquid Denmark, Ballerup, Denmark) was used as carrier gas while pure oxygen (N45, standard purity: 99.995%, Air-Liquid Denmark) served as the test gas. Inlet pressure was set to four bar at the regulator. WV permeability was measured using a PBI-Dansensor L80-5000 test instrument (Ringsted, Denmark) at 38°C and 90% RH. At least three replicate tests of each type were performed on each film.

RESULTS AND DISCUSSION

PLA masterbatch molecular weights

To optimize masterbatch synthesis of PLA in the presence of Cloisite® 30B, initial screening experiments were carried out in the range of 10–60 wt % clay loading. As shown in Table II (experiments 1–5), the initial conditions selected were [L]/[C] = 500 and 160°C. From these experiments, it was clear that PLA molecular weight decreased with increased clay loading. This might be explained by impeded polymer chain mobility in the proximity of clay particles at high loadings. Alternatively, impurities such as residual interlayer water present in the clay could also have a negative effect at higher clay loadings. Comparing experiments 5, 6, and 7, the results imply that PLA molecular weight increases with

TABLE II
GPC Analysis of PLA Nanocomposite Masterbatches

Experiment	L-lactide (g)	Clay/loading (%)	ROP temp. (°C)	[L]/[C]	M_w (Da)	M_n (Da)	PDI
1	5	–	160	500	94,800	39,000	2.4
2	5	C30B/10	160	500	33,800	19,900	1.7
3	5	C30B/20	160	500	13,500	8,000	1.7
4	5	C30B/40	160	500	11,800	7,000	1.7
5	5	C30B/60	160	500	10,700	6,700	1.6
6	5	C30B/50	160	1000	2,200	1,500	1.5
7	5	C30B/50	160	200	21,500	12,000	1.8
8	50	C30B/50	160	500	7,500	5,400	1.4
9	300	C30B/50	160	200	5,300	3,800	1.4
10	310	C30B/50	160	200	5,020	5,600	1.2
11	120	LDH-C_{12}/50	130	200	1,000	1,000	1.0

Note: C30B, Cloisite® 30B; PDI, polydispersity index.

decreasing lactide/catalyst ratio. This observation is in contrast to experience with living ring-opening polymerization of L-lactide[44,45] and might be explained by the presence of trace quantities of water in the clay or by increased viscosity as clay loading increases, which could lead to a reduced rate of catalyst diffusion. On the basis of further initial studies (experiments 8–10), and even though polymer molecular weights were further reduced, we decided to use [L]/[C] = 200 for preparation of PLA/Cloisite® 30B masterbatches and the same conditions were applied for PLA/LDH-C_{12} masterbatch generation. Although, as indicated in Table II, PLA molecular weights in the masterbatches (experiments 8–11) were quite low, this was not regarded as a very significant drawback because of the planned 10 : 1 dilution of each masterbatch with reference PLA granulate of much higher molecular weight to obtain final materials with ~ 5% clay loadings.

Extruded PLA and PLA nanocomposite molecular weights

The results from molecular weight analyses on PLA reference granulate, extruded pellets and extruded films are shown in Table III. The number-average molecular weight (M_n) of PLA decreased by ~ 7% when PLA-G was converted into film. Since M_n values measured in this way are, by estimation, only accurate to ±10%, such a change is probably not significant in real terms. Processing of PLA-G to PLA-P pellets resulted in a ~ 15% reduction in M_n; however, the resulting PLA-PF film exhibited virtually the same M_n. Dispersion of Cloisite® 30B directly in PLA as PLA-P1 or via masterbatch as PLA-P2 pellets produced films with M_n values very similar to those recorded for unfilled PLA film (PLA-PF) and therefore Cloisite® 30B addition at ~ 5 wt % did not adversely affect PLA during melt processing. In contrast, analysis of the extruded PLA-P3 pellets prepared by direct mixing of PLA and LDH-C_{12} showed a 75% reduction in M_n. As a result, these pellets produced a very low viscosity melt and continuous films could not be extruded. However, on dilution of PLA-P3 pellets by a factor of three with unprocessed PLA-G granulate, a continuous film identified as PLA-PF3-1 was produced with an estimated LDH loading of 1.8% and M_n of 55,400 Da.

There could be several reasons why PLA should degrade significantly when melt processed with LDH-C_{12}. First, although well dried before use, any traces of water released from this nanofiller could degrade PLA during processing into pellets. Second, Al and Mg metal coordinated sites on the LDH-C_{12} surface might catalyze PLA degradation. In this respect, it is notable that alkaline earth metal-based oxides and hydroxides have previously been described as selective catalysts for depolymerization of high-molecular weight PLA into L-lactide.[46–48] Furthermore, compounds of various metals such as Sn, Al, Fe, Ca, and Mg can affect PLA degradation behavior as noted by a number of researchers.[46,49–55] It is therefore possible that LDH-C_{12} dispersed in PLA might also act as a depolymerization catalyst leading to the very significant PLA molecular weight reduction which was observed.[56]

TABLE III
GPC Analysis of PLA Granulates, Processed Pellets and Films

Trial	Sample code	M_w (Da)	M_n (Da)	PDI
1	PLA-G	193,000	118,000	1.6
2	PLA-GF	186,600	110,900	1.7
3	PLA-P	178,100	101,200	1.7
4	PLA-PF	165,300	99,600	1.7
5	PLA-P1	168,900	101,800	1.6
6	PLA-PF1	153,900	98,300	1.6
7	PLA-P2	181,500	106,600	1.7
8	PLA-PF2	157,300	97,600	1.6
9	PLA-P3	50,800	25,300	2.0
10	PLA-PF3	50,700	25,700	2.0
11	PLA-PF3–1	116,800	55,400	2.1
12	PLA-P4	123,400	60,900	2.0
13	PLA-PF4	108,400	61,900	1.8
14	PLA-PF4–1	151,600	90,100	1.7

When LDH-C_{12} was dispersed from a masterbatch to obtain PLA-P4 pellets, it was possible to extrude a film (PLA-PF4) and although PLA in this film also had a significantly reduced M_n, this reduction was much less than that observed in PLA-PF3. This may have occurred because any residual water in LDH-C_{12} was consumed during masterbatch preparation. However, we cannot exclude the possibility that metal sites on LDH surfaces were modified by growing PLA chains during preparation of the masterbatch. Such modification could be due to grafting of growing PLA chains on the Al and Mg hydroxyl sites on the LDH surfaces during masterbatch production. This would effectively block sites which could otherwise catalyze PLA degradation.

Thermogravimetric analysis

As shown in Figures 1 and 2, both thermal degradation weight loss (TG) and the derivative plot of this weight loss (DTGA) were used to estimate the clay loading present in each nanocomposite. To achieve this objective, we compared the thermal properties of the individual components. In considering the thermal behavior of Cloisite® 30B, it was instructive to understand how the corresponding unmodified MMT (Cloisite® Na^+) behaves. As observed by Vázquez et al.,[57] Cloisite® Na^+ only loses ~ 3.5% in weight when heated to 400°C, probably as a result of water loss from surfaces or from the clay interlayer. In contrast, as shown in Figures 1 and 2,

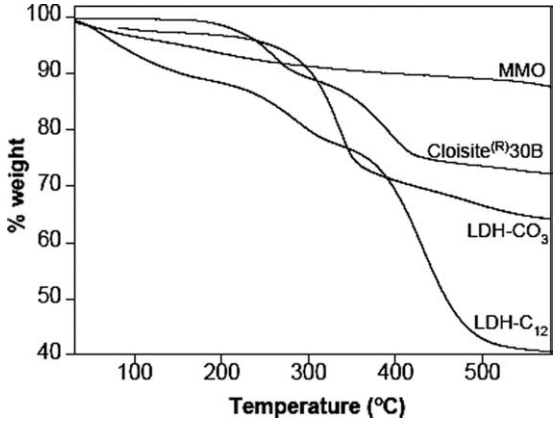

Figure 1 Thermal degradation of MMO, LDH-CO_3, LDH-C_{12}, and Cloisite® 30B clay.

weight loss in Cloisite® 30B occurs at 259°C and 393°C, which is attributed to decomposition of the organomodifier in a physically adsorbed form or in the interlayer spacing.[57] Cloisite® 30B showed ~ 25.8% weight loss at 470°C. Peeterbroeck et al.[58] estimated the organomodifier content in Cloisite® 30B to be 20.3% and the difference between this value and the weight loss determined here is likely due to the water content. Using the figure of 20.3% organomodifier in Cloisite® 30B, it can be estimated from the TGA data that the Cloisite® 30B loading in PLA-P1 and PLA-P2 was 4.5% and 5.3%, respectively. A similar method was used to estimate the actual LDH-C_{12} loading in PLA/LDH-C_{12} pellets. LDH-C_{12} showed three distinct peaks in the DTGA plot. These peaks can be assigned to loss of moisture below 180°C, decomposition of the laurate organomodifier in the range up to ~ 335°C and, thereafter, dehydration associated with the peak at ~ 450°C. In this case, it is difficult to estimate clay content by considering individual component weight losses as many phenomena take place simultaneously, especially at the higher temperatures. However, estimation of LDH-C_{12} content was possible by comparing

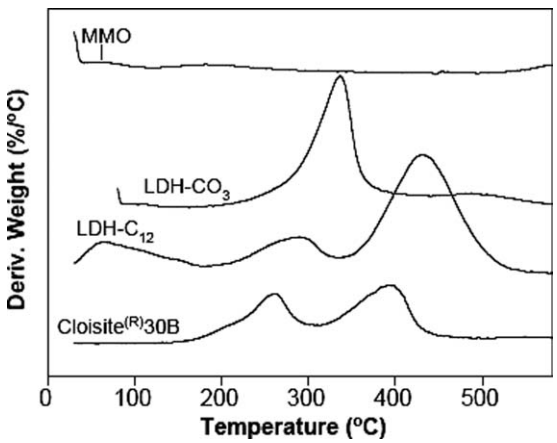

Figure 2 Derivative plot of thermal degradation (DTGA) of MMO, LDH-CO_3, LDH-C_{12}, and Cloisite® 30B clay.

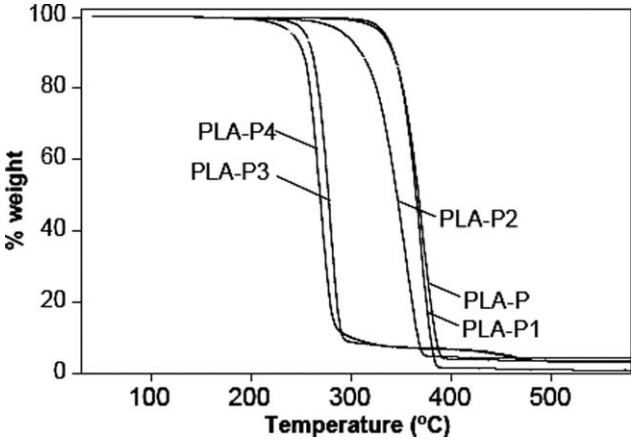

Figure 3 Thermal degradation of PLA and PLA-nanocomposite pellets.

Figures 1 and 3 at 580°C. At this temperature, residual weights of LDH-C_{12}, PLA-P, PLA-P3, and PLA-P4 were 40.6%, 0.86%, 3.03%, and 3.11%, respectively. Comparing the residual weight of PLA-P3 and PLA-P4 with PLA-P indicates that 2.17% and 2.25% MMO is present after combustion of PLA-P3 and PLA-P4, respectively. Finally, considering the relationship between starting weight of LDH-C_{12} and final yield of MMO at 580°C (Fig. 1) yielded an estimated loading of LDH-C_{12} of 5.3% and 5.5% for PLA-P3 and PLA-P4, respectively.

The degradation onset temperature of PLA-P (330°C) was comparable with that of PLA-P1 (330°C) but higher than that of PLA-P2 (310°C). This may be due to the presence of relatively low molecular weight PLA chains in the Cloisite® 30B masterbatch (Table II, experiments 8 and 9).

As shown in Figure 3, pellets PLA-P3 and PLA-P4 containing LDH-C_{12} are much less thermally stable than either PLA-P or the pellets containing Cloisite® 30B, which is consistent with the reduced M_n values indicated in Table III. Reduction in the thermal stability of LDH-based pellets is consistent with reports that metal oxides (e.g., MgO) lower the PLA degradation temperature.[46] Another report suggests that metal hydroxide (e.g., $Mg(OH)_2$) structures can cause random degradation of PLA, producing oligomers with active end groups along with formation of L-lactide due to the presence of MgO, resulting in a sharp decrease in thermal stability.[59] It should be noted, however, that the film extrusion temperatures used in the experiments reported here were significantly below the recorded degradation onset temperatures for PLA-P3 and PLA-P4.

Differential scanning calorimetry

The second heating scans in the DSC thermograms of PLA and PLA/clay films are shown in Figure 4.

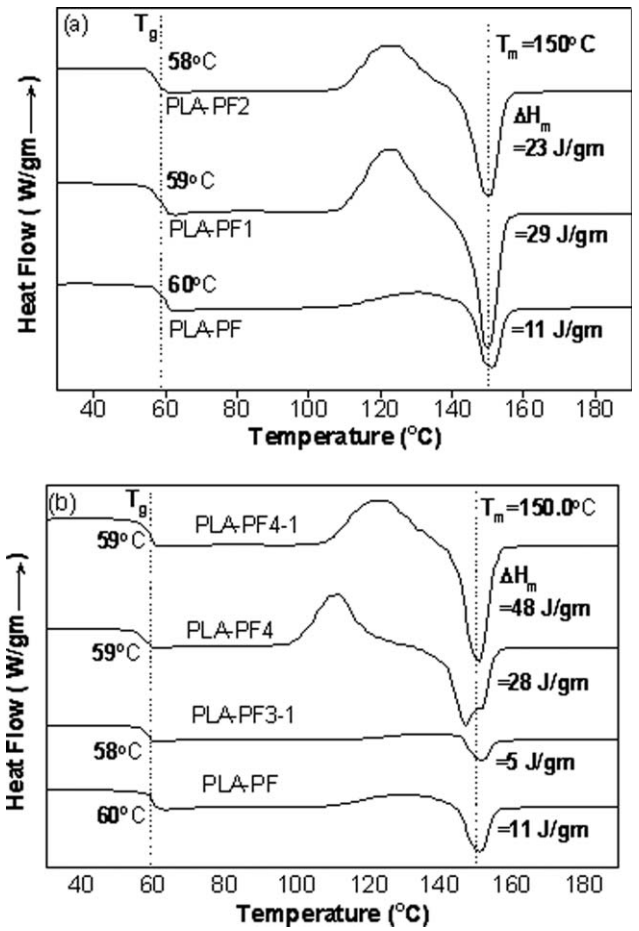

Figure 4 DSC second heating cycle scans for: (a) PLA/Cloisite® 30B nanocomposite films, (b) PLA/LDH-C_{12} nanocomposite films.

Notably, the T_g values are very similar in all cases. This is perhaps not surprising in the case of films containing Cloisite® 30B because of the minimal effect this additive has on PLA molecular weight.[60] In the case of films containing LDH-C_{12} with significantly reduced molecular weight, interactions between PLA chains and LDH surfaces could reduce the available free volume resulting in restricted PLA chain mobility. If this mechanism is in effect, such interactions could counteract effects due to the reduction in PLA molecular weight and lead to films with T_g values similar to that of unfilled PLA film. Table IV shows that, with the exception of PLA-PF3-1, the melting enthalpy (ΔH_m) increased in the PLA/clay compounds relative to unfilled PLA regardless of whether Cloisite® 30B or LDH-C_{12} was used. When comparing the full-width half-maximum values (FWHM) at T_m in Table IV, both PLA/Cloisite® 30B and PLA/LDH-C_{12} nanocomposite films yield very slightly narrower peak widths, which may suggest the formation of more uniform crystal sizes compared to unfilled PLA films. In the case of PLA-PF4, this observation is consistent with a broad distribution of crystallites and lower overall crystallinity, which could be explained by inhomogeneous distribution of crystallites, both in the bulk and in the vicinity of the LDH platelets. In the literature, it is reported that the crystallinity and size of the crystalline domains can decrease once organoclay addition exceeds a certain level.[14] This would explain why PLA-PF4-1 yielded higher crystallinity than PLA-PF4. In addition, from Table IV it is notable that PLA-PF4-1 film, containing an estimated 1.8% LDH-C_{12}, is significantly more crystalline than either unfilled PLA film, PLA-PF1, or PLA-PF2 films containing Cloisite® 30B at loadings of 4.5% or 5.3%. These findings may arise because LDH-C_{12} has a strong nucleation tendency when dispersed from a masterbatch at an optimum loading, yielding more uniform crystal sizes.

Optical polarimetry

As shown in Table V, the optical purity (OP) and mole fraction of D-lactyl units (X_D) did not change significantly during processing of PLA granulates into film. This was also the case for PLA films in which Cloisite® 30B was incorporated by direct mixing with PLA granulates. However, the OP value was lower in films containing Cloisite® 30B prepared using the masterbatch technique. A reduction in OP may arise because of interference from residual tin-based catalyst during processing. A similar effect was noticed when LDH-C_{12} was added directly into the PLA granulate before extrusion. In contrast, the OP increased in

TABLE IV
Summary of DSC Second Heating Cycle Data for PLA and PLA Nanocomposite Films

Samples	T_g (°C)	T_{cc} (°C)	ΔH_{cc} (J/g)	T_m (°C)	ΔH_m (J/g)	% X_c	FWHM of ΔH_m
PLA-PF	60	129	10	151	11	12	0.38
PLA-PF1	59	122	26	150	29	34	0.31
PLA-PF2	58	122	21	150	23	26	0.35
PLA-PF3–1	58	134	2	151	5	6	0.27
PLA-PF4–1	59	123	47	151	48	57	0.27
PLA-PF4	59	107	27	147, 152	28	31	0.48

T_g, glass transition temperature; ΔH_{cc}, enthalpy of cold crystallization; T_m, melting temperature; % X_c, percent crystallinity; FWHM, full-width half-maximum; T_{cc}, cold crystallization temperature.

TABLE V
Optical and Molecular Purity of PLA and PLA Clay Nanocomposite Film Samples

Sample code	$[\alpha]_{589}^{25}$	St. dev. $[\alpha]_{589}^{25}$	OP (%)	X_D
PLA-G	−148.13	0.27	95	0.025
PLA-PF	−149.19	0.58	96	0.022
PLA-PF1	−148.08	0.39	95	0.025
PLA-PF2	−141.25	0.58	91	0.047
PLA-PF3–1	−140.18	0.38	90	0.051
PLA-PF4–1	−152.67	0.22	98	0.011

$[\alpha]_{589}^{25}$, specific rotation; St. dev., standard deviation; OP, optical purity (%-L content); *XD*, mole fraction of D-lactyl units.

PLA-PF4-1, which was based on LDH-C_{12} inclusion using the masterbatch method followed by dilution with pure PLA. Differences in the optical purity of PLA/LDH-C_{12} nanocomposite films depending upon method of preparation may be associated with degradation of PLA during processing.[56] It is notable from Tables IV and V that the crystallinity of the PLA films increased with decreasing D-lactyl content, a trend that is in line with previous reports.[61] The literature indicates that PLA exhibits amorphous behavior if X_D ranges from 0.14 to 0.83.[42] From the data reported in Table V, it is possible that racemization may partly contribute to the low crystallinity of PLA-PF3-1 reported in Table IV.

Transparency

PLA film transparency is influenced by crystallinity and hence by processing conditions. Film extruded

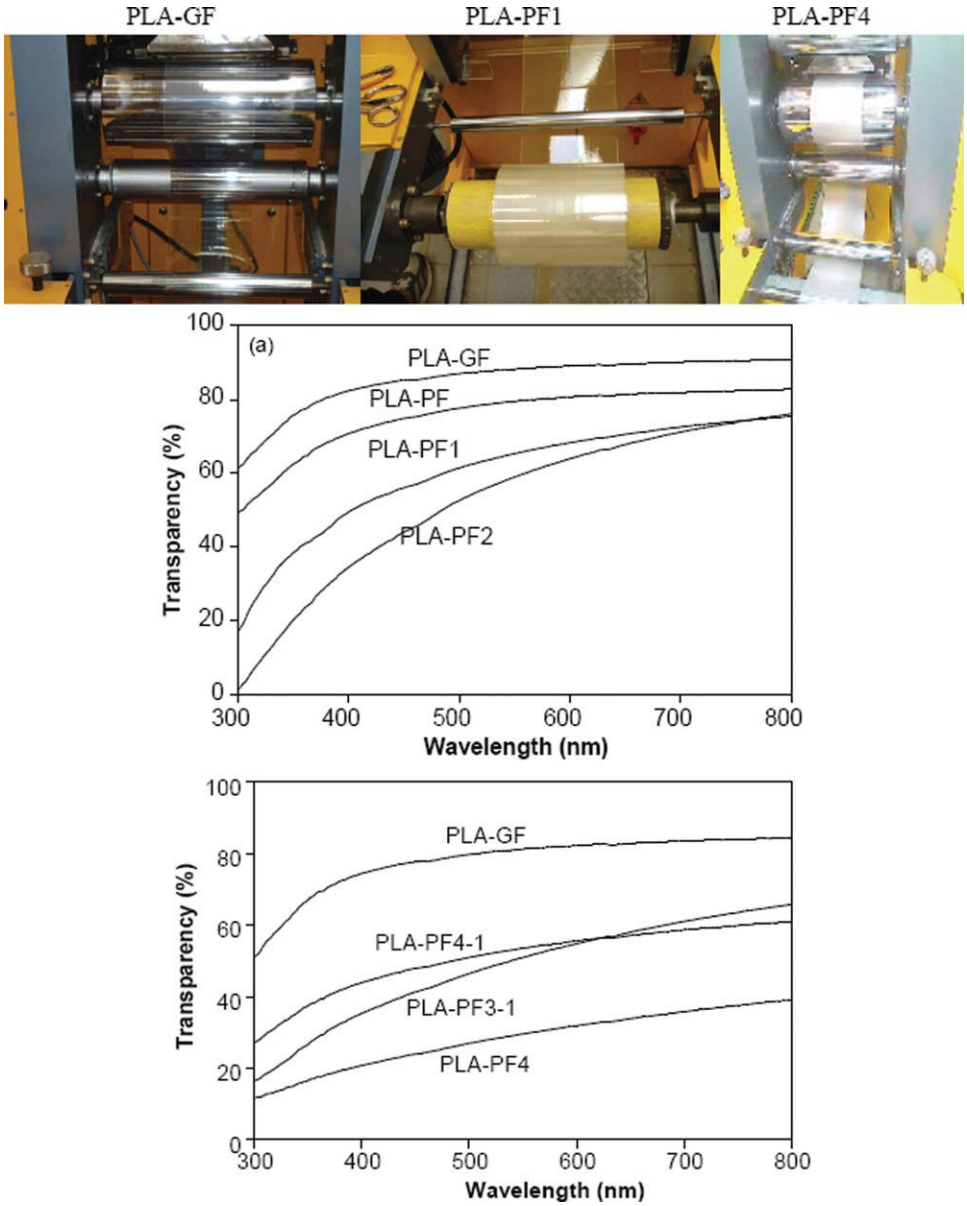

Figure 5 UV/visible spectra for (a) PLA/Cloisite® 30B films, (b) PLA/LDH-C_{12} films. [Color figure can be viewed in the online issue, which is available at wileyonlinelibrary.com.]

from the unprocessed PLA granulate (PLA-GF) yielded the highest transparency, but this decreased when the PLA-PF film was prepared from processed PLA-P pellets [Fig. 5(a)]. Transparency was further reduced in PLA-PF1 and PLA-PF2 films containing Cloisite® 30B and even more so in the case of films containing LDH-C_{12} [Fig. 5(b)]. It is possible that in addition to the quality of dispersion, the crystallization effects of the LDH nanofiller influenced the transparency of the films.

Morphology of PLA nanocomposite films by XRD analysis

Figure 6(a) shows the XRD pattern for Cloisite® 30B, with a peak at $2\theta = 5.75^\circ$ corresponding to an interlayer spacing $d_{001} \sim 1.8$ nm. This peak did not appear in XRD diffractograms for trial masterbatches containing 20 or 40% Cloisite® 30B loadings. However, evidence of this peak can be seen in the 60% loading Cloisite® 30B masterbatch along with another peak at $2\theta \sim 2.8^\circ$ corresponding to $d_{001} \sim 3.7$ nm, which suggests a combination of agglomeration and intercalation of PLA within Cloisite® 30B. Partly on the basis of these findings, 50% Cloisite® 30B clay loading was selected as an optimum for 300 g masterbatch production. As shown in Figure 6(b), films produced by diluting a PLA/Cloisite® 30B masterbatch into PLA-PF2 containing 5.3% clay showed a peak at $2\theta = 3.3^\circ$ corresponding to a basal spacing of 3.1 nm, suggesting an intercalated morphology. The XRD pattern for PLA-PF1 also shows a shift of the clay basal peak (d_{001}) from ~ 1.8 to ~ 3.1 nm. However, the intensity of the peak for PLA-PF1 is significantly lower than that of the peak for PLA-PF2, which could be due to a lower concentration of intercalated Cloisite® 30B particles. This observation may also indicate greater exfoliation of Cloisite® 30B in PLA-PF1 as compared to PLA-PF2. In general, the XRD results are consistent with a mixed exfoliated/intercalated morphology regardless of whether the PLA/Cloisite® 30B extruded films were prepared by direct addition or from masterbatch.

The XRD diffractogram of LDH-C_{12} shows a peak at $2\theta = 3.83^\circ$ indicating a basal spacing of $d_{001} \sim 2.65$ nm. This undispersed LDH-C_{12} peak was not observed in the films prepared either by direct mixing (PLA-PF3-1) or masterbatch (PLA-PF4 and PLA-PF4-1) techniques. This might suggest the exfoliation of LDH-C_{12} platelets. Furthermore, we observed a new peak at $2\theta \sim 11.65^\circ$ corresponding to an LDH interlayer spacing of 0.88 nm in PLA-PF4 and PLA-PF4-1 films. On the basis of discussion in the literature, this observation could be consistent with the presence of low molecular weight polylactide oligomers intercalated in the LDH interlayer structure.[62] Although, the possibility that laurate anions might leach out from organomodified LDH in the masterbatch, with subsequent formation of agglomerates, cannot be ruled out.

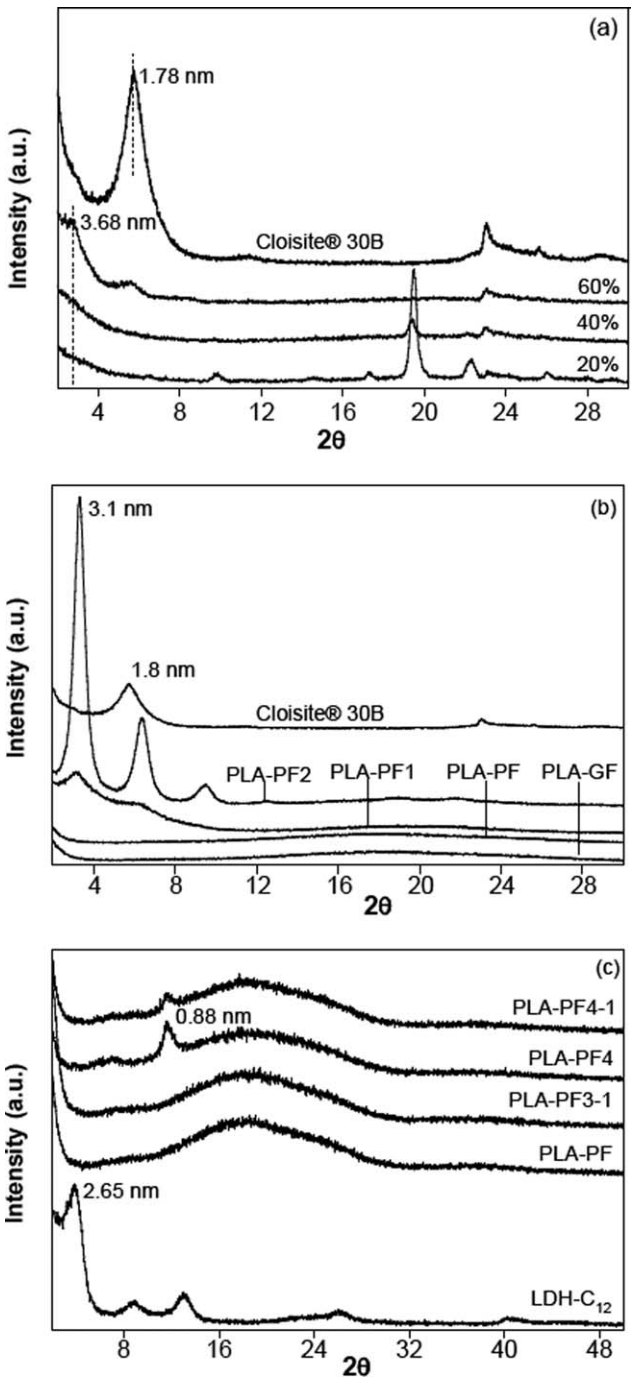

Figure 6 X-ray diffractograms for (a) Cloisite® 30B and Cloisite® 30B-based masterbatches, (b) PLA granulate and pellet reference films, PLA films containing 5% Cloisite® 30B and Cloisite® 30B, and (c) PLA pellet reference film and PLA films containing LDH-C_{12}.

Morphology of PLA nanocomposite films by TEM analysis

The TEM photographs shown in Figure 7(a,b) are representative images of PLA-PF1 and PLA-PF2

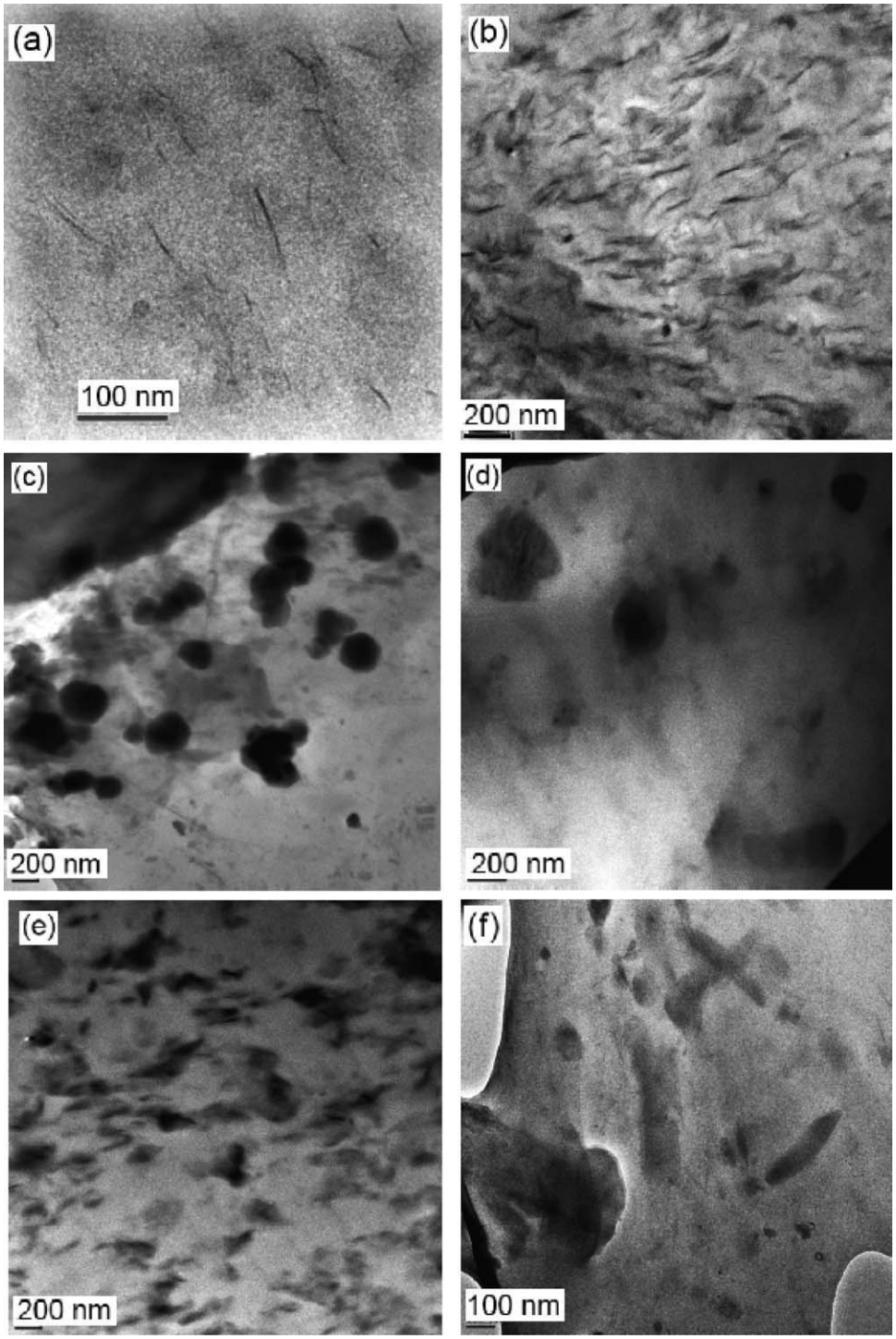

Figure 7 TEM images for (a) PLA-PF1, (b) PLA-PF2, (c) PLA-PF3, (d) PLA-PF3-1, (e) PLA-PF4, and (f) PLA-PF4 at higher magnification.

films, respectively. In these images the dark lines indicate the clay platelet dispersion and the lighter areas represent the PLA matrix. In PLA-PF1, more exfoliated Cloisite® 30B clay platelets are observed [Fig. 7(a)]; however, intercalated PLA-Cloisite® 30B platelets are also seen in the TEM images of both PLA-PF1 and PLA-PF2 [Fig. 7(a,b)]. These observations are consistent with the XRD analyses which, from the *d*-spacing of $\sim$ 3 nm, point to some degree of polymer intercalation in the clay galleries.

Figure 7(c) shows the TEM image of PLA-PF3 indicating the dispersion of LDH-C_{12} at 5.3% loading in the film. Although the material did not yield a continuous film, through examination of small samples we were able to visualize the dispersion of hexagonal platelets of LDH-C_{12}. Some of the platelets in

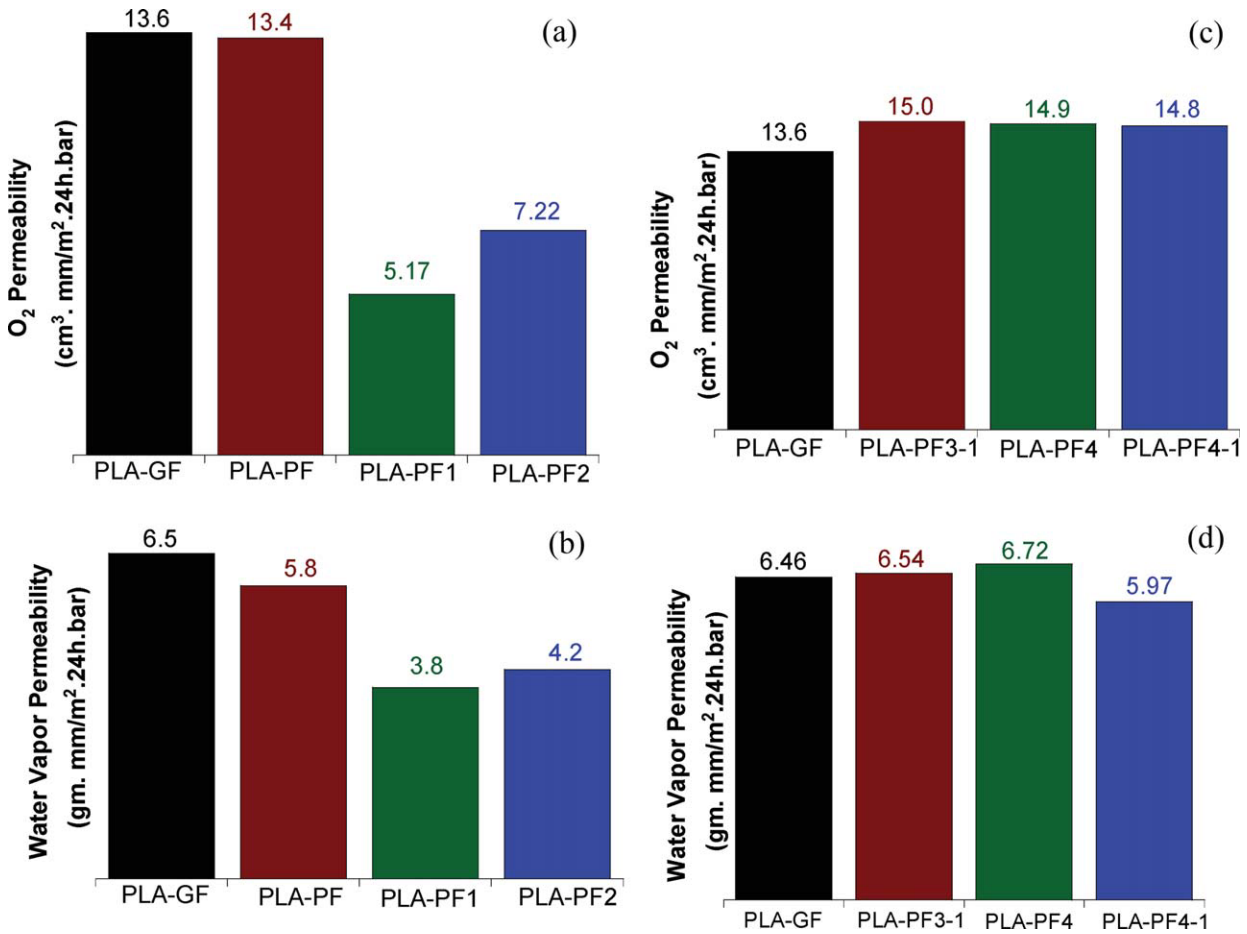

Figure 8 Oxygen permeability at 23°C and 50% RH and WV permeability at 38°C and 90% RH for PLA and PLA nanocomposite films: (a) O_2: unfilled PLA and PLA/Cloisite® 30B film, (b) WV: unfilled PLA and PLA/Cloisite® 30B film, (c) O_2: unfilled PLA and PLA/LDH-C_{12} film, (d) WV: unfilled PLA and PLA/LDH-C_{12} film. [Color figure can be viewed in the online issue, which is available at wileyonlinelibrary.com.]

this case are larger than 300 nm. Figure 7(d) shows further dilution of the LDH-C_{12} platelets in PLA-PF3-1 in which the filler loading is reduced to 1.8%. Figure 7(e) suggests that uniform dispersion of LDH-C_{12} has been achieved when using the prepared masterbatch; however, on the other hand, Figure 7(f) shows that LDH-C_{12} platelet agglomeration can also occur.

Film permeability

The measured oxygen and WV permeabilities of the various PLA and PLA nanocomposite films are presented in Figure 8(a–d). Neat PLA films either processed directly from the raw granulates or from extruded PLA pellets [Fig. 8(a)] yielded similar oxygen permeabilities (≈13.6 cm^3 mm/m^2 24 h bar). Addition of 4.5 wt % Cloisite® 30B in PLA films reduced the oxygen permeability by 47–62% depending upon how the filler was dispersed. Similarly, WV permeability was reduced by 39–41% [Fig. 8(b)]. In contrast, PLA/LDH-C_{12} films showed no reduction in either oxygen or WV permeability [Fig. 8(c,d)], suggesting that PLA molecular weight reduction, possibly in combination with inadequate nanoscale LDH-C_{12} dispersion, overwhelmed any barrier-enhancing effect which might otherwise have been achieved through LDH addition. The possibility that LDH platelets are too thin (∼ 0.7 nm) and too fragile to withstand shear forces during extrusion processing may also partly explain the lack of enhanced barrier properties in this case.

CONCLUSIONS

PLA-clay compounds were prepared and processed into films using either an organomodified LDH (LDH-C_{12}) or commercial organically modified MMT clay (Cloisite® 30B). In contrast to the findings with Cloisite® 30B, the use of the organomodified LDH resulted in a very significant reduction in polymer molecular weight after processing. This effect was

still significant but somewhat reduced when utilizing a previously prepared PLA/LDH-C_{12} masterbatch rather than direct blending of PLA/LDH-C_{12} in the extruder. This phenomenon, which occurred despite rigorous drying procedures, may have arisen either by release of water from within the LDH and/or as a result of the catalytic activity of metal sites on the LDH platelet surfaces. Consistent with this reduction in PLA molecular weight, the polymer degradation onset temperature was reduced when LDH-C_{12} was present as a nanofiller; however, this thermal degradation took place at temperatures above those to which the polymer was exposed during processing into film. Significantly higher PLA crystallinity was observed when films were prepared from PLA/LDH-C_{12} masterbatch, suggesting a strong nucleation tendency for this nanofiller. However, as indicated from optical analyses, racemization leading to increased D-lactyl content may also contribute to changes in PLA crystallinity as measured by DSC. A combination of XRD and TEM analyses pointed to exfoliated/intercalated morphologies in both PLA/Cloisite® 30B films and PLA/LDH-C_{12} films; however, in the latter case agglomerates were also observed. The transparency of the PLA films was compromised by addition of either filler, but this was more evident when LDH-C_{12} was used. Both oxygen and WV permeability were reduced significantly in the films containing $\sim$ 5.0% Cloisite® 30B, but barrier properties were not improved in any of the films containing LDH-C_{12}, which might be a result of PLA degradation counteracting any otherwise beneficial physical effects arising from the presence of LDH platelets in the polymer matrix. The findings presented here have identified difficulties in processing an organomodified LDH with PLA. A complete understanding of the mechanisms involved and the use of alternative LDH organomodifiers, which might circumvent the problems with PLA degradation during processing, remains the subject of continuing research.

We express sincere gratitude to Carina Gejl Nielsen, Færch Plast A/S and Stine Lausten, Kunststof-Kemi A/S for access to and assistance with the plastics processing equipment described in this article.

References

1. Dorgan, J. R.; Williams, J. S.; Lewis, D. N. J Rheol 1999, 43, 1141.
2. Auras, R.; Harte, B.; Selke, S. Macromol Biosci 2004, 4, 835.
3. Sudesh, K.; Iwata, T. Clean-Soil Air Water 2008, 36, 433.
4. Kawashima, N. J Synth Org Chem Jpn 2003, 61, 496.
5. Bordes, P.; Pollet, E.; Avérous, L. Prog Polym Sci 2009, 34, 125.
6. Zeng, Q. H.; Yu, A. B.; Lu, G. Q.; Paul, D. R. J Nanosci Nanotechnol 2005, 5, 1574.
7. Plackett, D. V.; Holm, V. K.; Johansen, P.; Ndoni, S.; Nielsen, P. V.; Sipilainen-Malm, T.; Sodergard, A.; Verstichel, S. Packag Tech Sci 2006, 19, 1.
8. Drumright, R. E.; Gruber, P. R.; Henton, D. E. Adv Mater 2000, 12, 1841.
9. Datta, R.; Tsai, S. P. Fuels Chem Biomass 1997, 666, 224.
10. Datta, R.; Tsai, S. P.; Bonsignore, P.; Moon, S. H.; Frank, J. R. Fems Microbiol Rev 1995, 16, 221.
11. Schmidt, S. C.; Hillmyer, M. A. J Polym Sci Part B: Polym Phys 2001, 39, 300.
12. Tsuji, H.; Takai, H.; Saha, S. K. Polymer 2006, 47, 3826.
13. Krikorian, V.; Pochan, D. J. Chem Mater 2003, 15, 4317.
14. Krikorian, V.; Pochan, D. J. Macromolecules 2004, 37, 6480.
15. Ray, S. S.; Yamada, K.; Okamoto, M.; Ueda, K. Nano Lett 2002, 2, 1093.
16. Ray, S. S.; Okamoto, M. Prog Polym Sci 2003, 28, 1539.
17. Shibata, M.; Someya, Y.; Orihara, M.; Miyoshi, M. J Appl Polym Sci 2006, 99, 2594.
18. Okada, A.; Usuki, A. Macromol Mater Eng 2006, 291, 1449.
19. Ray, S. S.; Yamada, K.; Ogami, A.; Okamoto, M.; Ueda, K. Macromol Rapid Commun 2002, 23, 943.
20. Ray, S. S.; Yamada, K.; Okamoto, M.; Ueda, K. Polymer 2003, 44, 857.
21. Paul, M. A.; Delcourt, C.; Alexandre, M.; Degee, P.; Monteverde, F.; Rulmont, A.; Dubois, P. Macromol Chem Phys 2005, 206, 484.
22. Du, L. C.; Qu, B. J.; Meng, Y. Z.; Zhu, Q. Compos Sci Technol 2006, 66, 913.
23. Lee, W. D.; Im, S. S.; Lim, H. M.; Kim, K. J. Polymer 2006, 47, 1364.
24. Illaik, A.; Taviot-Gueho, C.; Lavis, J.; Cornmereuc, S.; Verney, V.; Leroux, F. Chem Mater 2008, 20, 4854.
25. Taviot-Gueho, C.; Leroux, F. In Structure and Bonding; Duan, X.; Evans, D. G., Eds.; Springer-Verlag: Berlin, 2006; vol.119, p 121.
26. Vaysse, C.; Guerlou-Demourgues, L.; Duguet, E.; Delmas, C. Inorg Chem 2003, 42, 4559.
27. Vieille, L.; Taviot-Gueho, C.; Besse, J. P.; Leroux, F. Chem Mater 2003, 15, 4369.
28. Wang, L.; Brazis, P.; Rocci, M.; Kannewurf, C. R.; Kanatzidis, M. G. Chem Mater 1998, 10, 3298.
29. Pan, P.; Zhu, B.; Dong, T.; Inoue, Y. J Polym Sci Part B: Polym Phys 2008, 46, 2222.
30. Chiang, M.-F.; Wu, T.-M. Adv Mater Res, Part 1: Multi-Functional Mater Struct 2008, 47–50, 415.
31. Dagnon, K. L.; Ambadapadi, S.; Shaito, A.; Ogbomo, S. M.; DeLeon, V.; Golden, T. D.; Rahimi, M.; Nguyen, K.; Braterman, P. S.; D'Souza, N. A. J Appl Polym Sci 2009, 113 ,1905.
32. Rhim, J. W.; Lee, J. H.; Ng, P. K. W. L. Food Sci Technol 2007, 40, 232.
33. Thellen, C.; Orroth, C.; Froio, D.; Ziegler, D.; Lucciarini, J.; Farrell, R.; D'Souza, N. A.; Ratto, J. A. Polymer 2005, 46, 11716.
34. Tsuji, H.; Okino, R.; Daimon, H.; Fujie, K. J Appl Polym Sci 2006, 99, 2245.
35. Bao, L.; Dorgan, J. R.; Knauss, D.; Hait, S.; Oliveira, N. S.; Maruccho, I. M. J Membr Sci 2006, 285, 166.
36. Zenkiewicz, M.; Richert, J. Polym Test 2008, 27, 835.
37. Chang, J.-H.; An, Y. U.; Sur, G. S. J Polym Sci Part B: Polym Phys 2003, 41, 94.
38. Komatsuka, T.; Kusakabe, A.; Nagai, K. Desalination 2008, 234, 212.
39. Siracusa, V.; Rocculi, P.; Romani, S.; Dalla Rosa, M. Trends Food Sci Technol 2008, 19, 634.
40. Miyata, S. Clays Clay Miner 1975, 23, 369.
41. Garlotta, D. J Polym Environ 2001, 9, 63.
42. Tsuji, H.; Ikada, Y. Macromolecules 1992, 25, 5719.
43. Chabot, F.; Vert, M.; Chapelle, S.; Granger, P. Polymer 1983, 24, 53.

44. Zhang, L.; Pratt, R. C.; Nederberg, F.; Horn, H. W.; Rice, J. E.; Waymouth, R. M.; Wade, C. G.; Hedrick, J. L. Macromolecules 2010, 43, 1660.
45. Dubois, P.; Jacobs, C.; Jerome, R.; Teyssie, P. Macromolecules 1991, 24, 2266.
46. Fan, Y. J.; Nishida, H.; Mori, T.; Shirai, Y.; Endo, T. Polymer 2004, 45, 1197.
47. Hattori, H. Mater Chem Phys 1988, 18, 533.
48. Liu, Y.; Wei, R. Q.; Wei, J.; Liu, X. N. Prog Chem 2008, 20, 1588.
49. Kopinke, F.-D.; Remmler, M.; Mackenzie, K.; Möder, M.; Wachsen, O. Polym Degrad Stab 1996, 53, 329.
50. Cam, D.; Marucci, M. Polymer 1997, 38, 1879.
51. Fan, Y. J.; Nishida, H.; Shirai, Y.; Endo, T. Polym Degrad Stab 2003, 80, 503.
52. Fan, Y. J.; Nishida, H.; Hoshihara, S.; Shirai, Y.; Tokiwa, Y.; Endo, T. Polym Degrad Stab 2003, 79, 547.
53. Nishida, H.; Mori, T.; Hoshihara, S.; Fan, Y. J.; Shirai, Y.; Endo, T. Polym Degrad Stab 2003, 81, 515.
54. Mori, T.; Nishida, H.; Shirai, Y.; Endo, T. Polym Degrad Stab 2004, 84, 243.
55. Abe, H. Macromol Biosci 2006, 6, 469.
56. Katiyar, V.; Gerds, N.; Koch, C. B.; Risbo, J.; Hansen, H. C. B.; Plackett, D. Polym Degrad Stab 2010, 95, 2563.
57. Vázquez, A.; Lopez, M.; Kortaberria, G.; Martin, L.; Mondragon, I. Appl Clay Sci 2008, 41, 24.
58. Peeterbroeck, S; Alexandre, M.; Nagy, J. B.; Moreau, N.; Destrée, A.; Monteverde, F.; Rulmont, A.; Jérôme, R.; Dubois, P. Macromol Symp 2005, 221, 115.
59. Motoyama, T.; Tsukegi, T.; Shirai, Y.; Nishida, H.; Endo, T. Polym Degrad Stab 2007, 92, 1350.
60. Shim, J. H.; Kim, E. S.; Joo, J. H.; Yoon, J. S. J Polym Sci 2006, 102, 4983.
61. Lim, L.-T.; Auras, R.; Rubino, M. Prog Polym Sci 2008, 33, 820.
62. Chiang, M.-F.; Wu, T.-M. Compos Sci Technol 2010, 70, 110.